Skin Lesion Images Classification Using New Color Pigmented Boundary Descriptors

Saeid Amouzad Mahdiraji
Faculty of Electrical & Computer Engineering
Babol Noshirvani University of Technology
Babol, Iran
amouzad.saeid@yahoo.com

Yasser Baleghi, Sayed Mahmoud Sakhaei
Faculty of Electrical & Computer Engineering
Babol Noshirvani University of Technology
Babol, Iran
y.baleghi@nit.ac.ir, smsakhaei@nit.ac.ir

***Abstract*— Computational methods play an important role in enhancing the diagnosis of the skin cancer. Melanoma is the most fatal type of skin cancers that causes significant number of deaths in recent years. In this paper, novel boundary features are introduced based on the color variation of the skin lesion images, acquired with standard cameras. Furthermore, to reach higher performance in melanoma detection, a set of textural and morphological features are associated with proposed features. Multilayer perceptron neural network is used as classifier in this work. Results analysis indicate that proposed feature set has the highest mean accuracy (87.80%), sensitivity (87.92%), specificity (87.65%) and precision (90.39%) in comparison with the previous works in Dermatology Information System (IS) and DermQuest datasets.**

Keywords*— Macroscopy; Pigmented boundary; Skin lesion; Melanoma; Feature extraction

I. INTRODUCTION

One of the most usual types of cancer in different countries is skin cancer, of which the incidence rate has increased during recent years [1]. Among all forms of skin cancers, melanoma is the deadliest one [2]. According to estimation of The American Cancer Society, in Unites States about 76380 new cases of melanoma will be diagnosed (46870 in men and 29510 in women) and about 10130 deaths from melanoma will occur (6750 in men and 3380 in women) in 2016 [3, 4].

Early diagnosis of skin disease helps clinicians and dermatologists to find exact signs and prevention approach of it [5]. Chance of curing in early diagnosed people is mostly higher than the others [6]. The present clinical standard for identifying skin lesions is visual examination. One of the most common approaches for detecting a skin lesion is the "ABCD" criteria that stand for asymmetry (A), border (B), color (C) and diameter (D) [7]. Nowadays Computational methods help dermatologists to analyze skin lesions in both macroscopic and dermoscopic images [1].

In this study, novel boundary features are suggested based on border color variation of skin lesions. Other studies often extract all asymmetry, border, color and diameter features. These features are obtained according to this fact that melanoma lesions mainly have various pigmented colors in contrast with non-melanoma lesions [8]. A brief survey of some recent papers on skin lesion diagnosis with emphasis on border characteristics are given in following and summarized in Table I.

Ma *et al* [9] used wavelet decomposition for analysis of the contour structural irregularity of skin lesions. Amelard *et al* [10] employed morphological high-level intuitive features (HLIFs) that measure border irregularity of skin lesions. These features are combined with modified feature set proposed by Cavalcanti *et al* [11]. Zhou *et al* [12] used a boundary characteristic descriptor which is called centroid distance diagram (CCD) to describe border irregularity of pigmented lesions. Garnavi *et al* [13] suggested 1) wavelet-based texture analysis; 2) geometrical measurements; and 3) boundary-series analysis in spatial and frequency domains to extract features. Clawson *et al* [14] described a harmonic-wavelet based methodology for skin lesion border evaluation.

Macroscopic images captured by standard camera, are more accessible and have less limitation rather than dermatoscope ones [15]. Therefore, we use macroscopic images for analyzing lesions.

A new feature set is proposed in this work based on color variation of boundary pixels of a lesion. These features are combined with other morphological and textural features to improve the classification results. The results of the classification are calculated for each feature set separately and compared with previous studies. The outcomes shows higher performance than the other related works with same datasets. Artificial neural network with a back propagation (BP) training algorithm is utilized as the classifier to determine the lesion type.

II. PROPOSED METHOD

Color variation of a skin lesion is an important criterion for dermatologists to discriminate malignant lesions from benign. Unlike melanoma lesions that tend to have various pigmented color distributions, benign nevi often have homogeneous color distributions [7]. Amelard *et al* [8] used this to extract color high-level intuitive features (HLIFs) from entire lesion. Pigmented boundary is a key discriminating factor between melanoma and non-melanoma

978-1-5090-6454-0/17/$31.00© IEEE

cases; however, no quantitative descriptor have been proposed by previous works to describe the irregularity of pigmentation of lesion

TABLE I. MAXIMUM CLASSIFICATION ACCURACY, SENSITIVITY AND SPECIFICITY RESULTS IN PREVIOUS STUDIES ON SKIN LESIONS CLASSIFICATION.

Ref. (year)	Features	Acc. (%)	Sen. (%)	Spe. (%)	Dataset
[9] (2013)	Boundary wavelet decomposition	-	83	90	134 Macro, Atlas database, Available at http://www.dermnet.com.
[10] (2012)	Morphological HLIFs + modified Cavalcanti *et al* feature set.	87.38	90.76	82.76	206 Macro, IS and DermQuest datasets.
[12] (2010)	CCD as boundary characteristic descriptor	-	74.2	72.6	167 Macro, local pigmented lesion clinics, was collected between November 2004 and October 2008.
[13] (2012)	Wavelet-based texture analysis, geometrical measurements and boundary-series analysis	91.26	-	-	289 Derm, NM
[14] (2009)	Harmonic-wavelet based methodology	93.30	90	-	30 Derm, Were captured using MoleMax™ and was collected between September 2005 and January 2007.

Ref: reference, Macro: macroscopic images, Derm: dermoscopic images, Acc: Accuracy, Sen: Sensitivity, Spe: Specificity, NM: non-mentioned, HLIFs: High-Level Intuitive Features, CCD: centroid distance diagram. Unreported results specified with dash mark.

borders. In this paper, two kinds of color-based features extracted from lesion borders are proposed.

A. Type I: Boundary color value differences

Malignant melanoma lesions mainly have varying color distribution in boundary pixels. Value difference from mean of each boundary pixel in a melanoma lesion is different from a non-melanoma lesion in each color channel. Mean square error (MSE) criteria (indicated in (1)) is used to compute the differences for a lesion in each color channel.

$$f^{I} = \frac{1}{N}\sum_{i=1}^{N}(V_i - V_m)^2, \quad i = 1,...,N \tag{1}$$

where N is the number of boundary pixels, V_i is value of ith boundary pixel and V_m is the mean value of boundary pixels for a lesion.

This feature is extracted in gray level, RGB, HSV, YCbCr, CIE L*a*b* [16], CMYK, L*C*H* [17] and CIEXYZ [17] color spaces. Consequently, 22 features are extracted in this part.

B. Type II: Boundary color clustering features

Six major lesion colors (white, red, light-brown, dark-brown, blue-gray, and black) are defined for skin lesions. Melanoma cases are usually exhibited in three or more colors [18]. Clustering the lesion with different k clusters and comparing the results, introduced color features that discriminate benign and malignant lesions [8]. In this study, clustering boundary pixels of a lesion is proposed. First original RGB image is transformed to intuitive uniform color space. CIE L*a*b space is used in [8] for this goal, where color values are considered according to approximate relative perceptual difference. K-means clustering using Euclidean distance is employed for clustering. K is set 1, 2 and 5 clusters. K=1 case is just utilized for comparison with other clusters. Standard camera images mainly include illumination artifacts leading to misclassification of main six colors [8]; Hence, maximum 5 clusters are considered for a lesion. A result example of abovementioned clustering is depicted in Fig. 1.

Four features are achieved from the clustering results which are given in equations (2) to (5).

$$f_1^{II} = \frac{1}{N}\sum_{i=1}^{N}(C_i^5 - C_i^1)^2, \quad i = 1,...,N \tag{2}$$

$$f_2^{II} = \frac{1}{N}\sum_{i=1}^{N}(C_i^5 - C_i^2)^2 \tag{3}$$

$$f_3^{II} = \frac{\left(\sum_{i=1}^{N}(C_i^5 - I_i)^2\right)}{\left(\sum_{i=1}^{N}(C_i^1 - I_i)^2\right)} \tag{4}$$

$$f_4^{II} = \frac{\left(\sum_{i=1}^{N}(C_i^2 - I_i)^2\right)}{\left(\sum_{i=1}^{N}(C_i^1 - I_i)^2\right)} \tag{5}$$

where N is number of boundary pixels, C^k_i is result of clustering with k clusters and I is the value of transformed boundary lesion pixels in L*a*b* space.

III. EXPERIMENTAL RESULTS

A. Dataset description

The dataset used in this study contains 206 images that were obtained using standard cameras. These images are categorized into two types: malignant melanoma and nevi. The same dataset is used in [8, 10, 19, 20]. The details are given below.

- Malignant melanoma: 119 images (43 from the Dermatology Information System (IS) [21] and 76 from DermQuest [22])
- Nevi: 87 images (26 from the Dermatology Information System and 61 from DermQuest)

Each image contains only a single lesion which is manually segmented to create binary area for distinguishing

lesion pixels from surrounding skin. That helps to analyze the feature extraction performance irrespective of an automatic segmentation accuracy. Four images from these datasets are shown in Fig. 2.

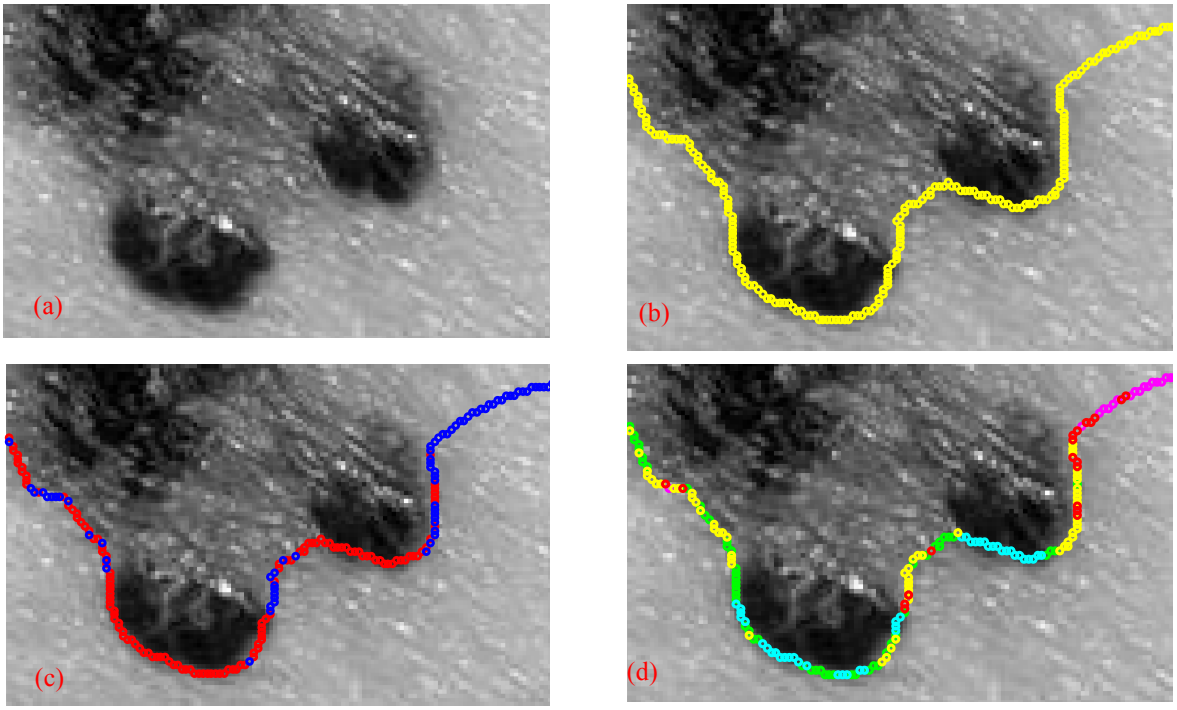

Fig. 1. A result example of boundary color clustering on close view of a melanoma lesion. Clustering results are colored for visualization purposes. Fig. (a) gray scale representation of a melanoma lesion. Figs. (b), (c) and (d) are boundary clustering with 1, 2 and 5 clusters, respectively.

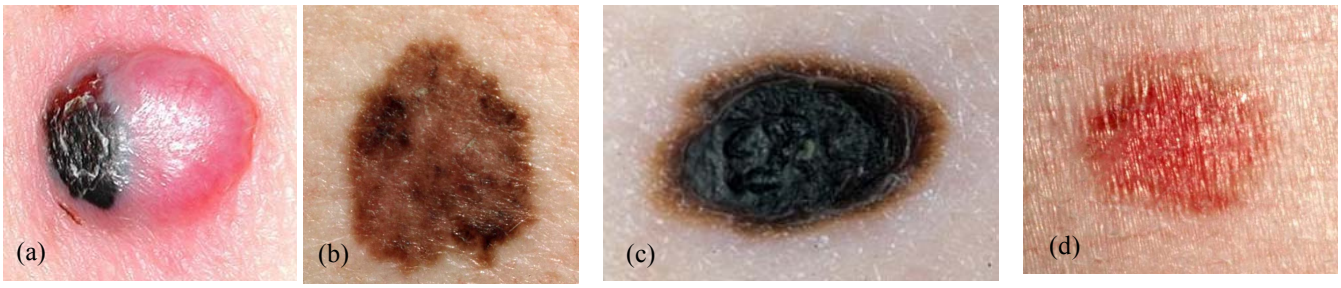

Fig. 2. Examples of IS dataset images (a, c) and DermQuest dataset images (b, d); a, b are melanoma and, c, d are nevi.

B. *Feature Extraction*

Boundary Features presented in section II, are calculated based on color variation of the lesion contour. Totally 26 novel features are extracted. We also use some other morphological and textural features [23] (that are employed for leaf images) to fuse with proposed features to enhance the accuracy of lesion recognition. The following notation describes various features used in this paper.

- ***Type I: Boundary color value differences***: set of 22 features describing value differences from their mean of each boundary pixel.
- ***Type II: Boundary color clustering features***: set of 4 color features that compare clustering of boundary pixels with different clusters.
- $\boldsymbol{F_P}$: set of 26 features containing all proposed features (see Section II).
- $\boldsymbol{F_C}$: set of 12 morphological and textural features [23].
- $\boldsymbol{F_T}$: set of 38 features attained by union of $\boldsymbol{F_P}$ and $\boldsymbol{F_C}$ ($\boldsymbol{F_T}=\boldsymbol{F_P}\cup\boldsymbol{F_C}$).

Yousefi proposed morphological and textural features [23] that are labeled as f_i and presented in the following.

- f_1: Lesion area to the convex area ratio

$$f_1 = \frac{S}{S_r} \tag{6}$$

where S is lesion area and S_r is area of the smallest rectangle that bounds the lesion shape.

- f_2: Maximum axis to the minimum axis ratio.

$$f_2 = \frac{d_{\max}}{d_{\min}} \quad (7)$$

where d_{max} and d_{min} are maximum and minimum axis of smallest bounding rectangle of the lesion, respectively.

- f_3: Bounding box length to bounding box width ratio.

$$f_3 = \frac{l_{\max}}{l_{\min}} \quad (8)$$

where l_{max} and l_{min} are length and width of the smallest bounding rectangle of the lesion, respectively.

- f_4: Circularity

$$f_4 = \frac{S}{S_b} \quad (9)$$

where S is lesion area and S_b is the area of the smallest circle that bounds the lesion shape.

- f_5: Lesion area to distance of left corner of bounding box from center of mass of the shape ratio.

$$f_5 = \frac{S}{l_{rb}} \quad (10)$$

where S is lesion area and l_{rb} is the distance of left corner of bounding box from center mass of the shape.

- f_6: Ratio of Sum of All Grey Scale Values of Lesion Image to Lesion Area.

$$f_6 = \frac{\left(\sum_{j=1}^{n}\sum_{i=1}^{m} f_{ij}\right)}{S} \quad (11)$$

where S is lesion area and f_{ij} is gray scale value of lesion image in (i,j) coordinates.

- f_7: Ratio of Lesion Area to Its Squared Perimeter.

$$f_7 = \frac{S}{P^2} \quad (12)$$

where S is lesion area and P is perimeter of the lesion.

- f_8: Perimeter to the Bounding Box Perimeter Ratio.

$$f_8 = \frac{P}{P_r} \quad (13)$$

where P is perimeter of the lesion and P_r is bounding box perimeter of lesion image.

- f_9, f_{10} and f_{11}: Sum of Lesion Pixels' HSV Values Normalized by Lesion Image Area.

$$f_9 = \frac{\left(\sum_{j=1}^{n}\sum_{i=1}^{m} h_{ij}\right)}{S} \quad (14)$$

$$f_{10} = \frac{\left(\sum_{j=1}^{n}\sum_{i=1}^{m} s_{ij}\right)}{S} \quad (15)$$

$$f_{11} = \frac{\left(\sum_{j=1}^{n}\sum_{i=1}^{m} v_{ij}\right)}{S} \quad (16)$$

where S is lesion area and h_{ij}, s_{ij} and v_{ij} are values of lesion image in (i,j) coordinates in HSV color space.

- f_{12}: A Nonlinear Combination of f_6 and f_{11}.

$$f_{12} = f_6^2 + f_{11}^2 \quad (17)$$

C. Normalization and Classification

After the feature extraction stage, all features are normalized using (18).

$$X_i^{norm} = \frac{X_i - X_{\min}}{X_{\max} - X_{\min}} \quad (18)$$

where X_i^{norm} is the normalized feature, X_i is the main feature and X_{min} and X_{max} are smallest and largest values of the main feature, respectively.

Then, the normalized features vector is applied to Multilayer Perceptron (MLP) neural network using back propagation algorithm for classification.

Images of each class (Melanoma and Nevi) were randomly split to 80%/20% train/test sets before training and testing algorithms. We used statistical measures accuracy, sensitivity, specificity and precision to evaluate performance, which is defined in equations (19) to (22).

$$\text{Accuracy} = \frac{TP + TN}{TP + FP + FN + TN} \quad (19)$$

$$\text{Sensitivity} = \frac{TP}{(TP + FN)} \quad (20)$$

$$\text{Specificity} = \frac{TN}{(TN + FP)} \quad (21)$$

$$\text{Precision} = \frac{TP}{(TP + FP)} \quad (22)$$

where TP, FP, TN and FN are the number of true positive (correct malignant estimation), false positive (incorrect malignant estimation), true negative (correct benign estimation) and false negative (incorrect benign estimation) cases, respectively.

TABLE II. COMPARISION OF BEST CLASSIFICATION RESULTS IN PREVIOUS STUDIES AND THIS WORK

Method	Number of features	Acc. (%)	Sen. (%)	Spe. (%)	Pre. (%)
[10]	51	87.38	90.76	82.76	-
[20]	54	86.89	91.60	80.46	-
F_P proposed	26	85.36	87.50	82.35	87.50
F_C proposed	12	87.80	91.67	82.35	88.00
F_T proposed	38	**92.68**	**95.83**	**88.23**	**92.00**

Acc: Accuracy, Sen: Sensitivity, Spe: Specificity, Pre: precision, F_P: proposed feature set, F_C: morphological and textural feature set, F_T: $F_P \cup F_C$.
Best results of each measure marked in boldface.
Unreported results specified with dash mark.

D. Results and Disussion

The combination of proposed feature set and morphological and textural features resulted in a 38-dimensional feature space. Each feature set was applied separately to the MLP neural network. Accuracy, sensitivity, specificity and precision of the NN classification are calculated for the each of the feature sets.

Several lesion diagnosis methods have been previously reported on IS and Dermquest datasets. We made a comparison between them and proposed feature sets according to the best results. The results are given in Table II.

According to Table II, concatenating the $\boldsymbol{F_P}$ and $\boldsymbol{F_C}$, enhances the lesion diagnosis rate. Moreover, classification using $\boldsymbol{F_T}$ obtains the highest accuracy (92.68%), sensitivity (95.83%), specificity (88.23%) and precision (92%) in comparison of the $\boldsymbol{F_P}$ and $\boldsymbol{F_C}$ and also previous works on these datasets.

To illustrate the robustness of the proposed features, classification is performed in 10 trials and the average of them is reported as results. The outcomes for all feature sets and previous works on these datasets are summarized in Table III.

As expected, $\boldsymbol{F_T}$ achieves the highest mean accuracy (87.80%), sensitivity (87.92%), specificity (87.65%) and precision (90.39%) in comparison with the previous works.

$\boldsymbol{F_T}$ also has lower feature dimension in comparison with previous works. Thus, this higher performance is obtained with less computational cost.

IV. CONCLUSION

The main aim of this study is to devise a novel feature set that improves the skin lesion images diagnosis. New sets of boundary features are proposed to describe the color variation of boundary lesion images acquired using standard cameras. Type I features describe the value differences of each boundary pixel from average of them in each color channel. Type II features compare clustering of boundary pixels with different clusters. Experimental results express that combining the proposed features with a set of 12 morphological and textural features and applying the data to the MLP neural network for classification, enhances the performance of the recognition. $\boldsymbol{F_T}$ feature set has lowest feature dimension and highest classification rate in comparison with the previous works on IS and Dermquest datasets.

Optimum features based on texture and shape of the lesions can be designed and concatenated with the proposed feature set of this study to achieve the higher performance. Also feature evaluation methods can be applied on the feature sets to attain the optimum results.

REFERENCES

[1] R. B. Oliveira, J. P. Papa, A. S. Pereira, and J. M. R. Tavares, "Computational methods for pigmented skin lesion classification in images: review and future trends," Neural Computing and Applications, pp. 1-24, 2016.

[2] A. F. Jerant, J. T. Johnson, C. Sheridan, and T. J. Caffrey, "Early detection and treatment of skin cancer," American family physician, vol. 62, pp. 357-386, 2000.

[3] R. L. Siegel, K. D. Miller, and A. Jemal, "Cancer statistics, 2016," CA: a cancer journal for clinicians, vol. 66, pp. 7-30, 2016.

[4] (2 Sep 2016). American Cancer Society (2016) Cancer facts & figures 2016. Available: http://www.cancer.org/research/cancerfactsstatistics/cancerfactsfigures2016/index

[5] O. Abuzaghleh, B. D. Barkana, and M. Faezipour, "Noninvasive real-time automated skin lesion analysis system for melanoma early detection and

TABLE III. COMPARISION OF MEAN AND STANDARD DEVIATION OF CLASSIFICATION RESULTS IN 10 TRIALS IN PREVIOUS STUDIES AND THIS WORK.

Method	Number of features	Acc. (%)		Sen. (%)		Spe. (%)		Pre. (%)	
		μ	σ	μ	σ	μ	σ	μ	σ
[8]	62	83.59	1.14	91.01	1.64	73.45	3.69	-	-
[24]	59	81.26	1.31	84.04	3.67	79.91	0.98	-	-
F_P proposed	26	81.71	2.07	84.58	2.81	77.56	2.48	84.24	1.63
F_C proposed	12	85.61	1.38	**90.00**	2.15	79.41	3.10	86.10	1.71
F_T proposed	38	**87.80**	3.25	87.92	4.98	**87.65**	1.86	**90.93**	1.45

Acc: Accuracy, Sen: Sensitivity, Spe: Specificity, Pre: precision, F_P: proposed feature set, F_C: morphological and textural feature set, F_T: $F_P \cup F_C$.
Best average results of each measure marked in boldface.
Unreported results specified with dash mark.

prevention," IEEE journal of translational engineering in health and medicine, vol. 3, pp. 1-12, 2015.
[6] O. Abuzaghleh, B. D. Barkana, and M. Faezipour, "SKINcure: A real time image analysis system to aid in the malignant melanoma prevention and early detection," in Image Analysis and Interpretation (SSIAI), 2014 IEEE Southwest Symposium on, 2014, pp. 85-88.
[7] F. Nachbar, W. Stolz, T. Merkle, A. B. Cognetta, T. Vogt, M. Landthaler, et al., "The ABCD rule of dermatoscopy: high prospective value in the diagnosis of doubtful melanocytic skin lesions," Journal of the American Academy of Dermatology, vol. 30, pp. 551-559, 1994.
[8] R. Amelard, J. Glaister, A. Wong, and D. A. Clausi, "High-level intuitive features (HLIFs) for intuitive skin lesion description," IEEE Transactions on Biomedical Engineering, vol. 62, pp. 820-831, 2015.
[9] L. Ma and R. C. Staunton, "Analysis of the contour structural irregularity of skin lesions using wavelet decomposition," Pattern recognition, vol. 46, pp. 98-106, 2013.
[10] R. Amelard, A. Wong, and D. A. Clausi, "Extracting morphological high-level intuitive features (HLIF) for enhancing skin lesion classification," in 2012 Annual International Conference of the IEEE Engineering in Medicine and Biology Society, 2012, pp. 4458-4461.
[11] P. G. Cavalcanti and J. Scharcanski, "Automated prescreening of pigmented skin lesions using standard cameras," Computerized Medical Imaging and Graphics, vol. 35, pp. 481-491, 2011.
[12] Y. Zhou, M. Smith, L. Smith, and R. Warr, "A new method describing border irregularity of pigmented lesions," Skin Research and Technology, vol. 16, pp. 66-76, 2010.
[13] R. Garnavi, M. Aldeen, and J. Bailey, "Computer-aided diagnosis of melanoma using border-and wavelet-based texture analysis," IEEE Transactions on Information Technology in Biomedicine, vol. 16, pp. 1239-1252, 2012.
[14] K. M. Clawson, P. Morrow, B. Scotney, J. McKenna, and O. Dolan, "Analysis of pigmented skin lesion border irregularity using the harmonic wavelet transform," in Machine Vision and Image Processing Conference, 2009. IMVIP'09. 13th International, 2009, pp. 18-23.
[15] H. C. Engasser and E. M. Warshaw, "Dermatoscopy use by US dermatologists: a cross-sectional survey," Journal of the American Academy of Dermatology, vol. 63, pp. 412-419. e2, 2010.
[16] C. CIE, "Commission Internationale de l'Eclairage Proceedings, 1931," ed: Cambridge University Press Cambridge, 1932.
[17] M. Celenk, "A color clustering technique for image segmentation," Computer Vision, Graphics, and image processing, vol. 52, pp. 145-170, 1990.
[18] N. M. Sirakov, Y.-L. Ou, and M. Mete, "Skin lesion feature vectors classification in models of a Riemannian manifold," Annals of Mathematics and Artificial Intelligence, vol. 75, pp. 217-229, 2015.
[19] R. Amelard, J. Glaister, A. Wong, and D. A. Clausi, "Melanoma decision support using lighting-corrected intuitive feature models," in Computer Vision Techniques for the Diagnosis of Skin Cancer, ed: Springer, 2014, pp. 193-219.
[20] R. Amelard, A. Wong, and D. A. Clausi, "Extracting high-level intuitive features (HLIF) for classifying skin lesions using standard camera images," in Computer and Robot Vision (CRV), 2012 Ninth Conference on, 2012, pp. 396-403.
[21] "Dermatology Information System," ed. http://www.dermis.net, 2012.
[22] "DermQuest," ed. http://www.dermquest.com, 2012.
[23] E. Yousefi, "Leaves Recognition for Plants Classification Using Elliptic Fourier Descriptor," Master of Science, Thesis, Electrical & Computer Engineering,, Babol Noshirvani University of Technology, 2015.
[24] R. Amelard, J. Glaister, A. Wong, and D. A. Clausi, "Melanoma decision support using lighting-corrected intuitive feature models," in Computer Vision Techniques for the Diagnosis of Skin Cancer, ed: Springer, 2014, pp. 193-219.